Journal of Water Process Engineering 21 (2018) 69–76

Contents lists available at ScienceDirect

Journal of Water Process Engineering

journal homepage: www.elsevier.com/locate/jwpe

Nano-hematite bagasse composite (*n*-HBC) for the removal of Pb(II) from dilute aqueous solutions

Meina Liang[a,b], Dunqiu Wang[a,b,*], Yinian Zhu[a,b], Zongqiang Zhu[b,c], Yanhong Li[b], C.P. Huang[c,**]

[a] College of Light Industry and Food Engineering, Guangxi University, Nanning 530004, PR China
[b] College of Environmental Science and Engineering, Guilin University of Technology, Guilin 541004, PR China
[c] Department of Civil and Engineering, University of Delaware, Newark, DE 19716, United States

ARTICLE INFO

Keywords:
Nano-hematite bagasse composite (*n*-HBC)
Lead(II)
Surface complex formation
Adsorption
Impregnation

ABSTRACT

Nano-hematite bagasse composite (*n*-HBC) was synthesized, characterized and tested for the removal of Pb(II) from dilute aqueous solutions. The particle size of ferric oxide was in the range of 100–300 nm. The composite surface, both internal and external, was occupied by abundant oxygen-containing functional groups. The optimum Pb(II) adsorption density occurred in the pH range from 4.0 to 5.5. Adsorption reached equilibrium rapidly in 480, 600, 720 min at initial Pb(II) concentration of 20, 30, and 40 mg/L, respectively, at 25 °C and pH 5.0. The maximum Pb(II) adsorption capacity, calculated from the Langmuir adsorption isotherm, was 16.57 mg/g at 25 °C. Furthermore, surface complexation model was also applied to describe the adsorption reaction between aqueous Pb(II) and *n*-HBC. The Gibbs free energy of adsorption, ΔG_{ads}^{0}, was −39.49 kJ/mol (9.44 kcal/mol) at 25 °C, which indicated spontaneous Pb(II) ion adsorption on *n*-HBC. Results of XPS studies demonstrated the presence of surface oxygen-containing functional groups, which were involved in the adsorption of Pb(II) and that hematite played a key role in Pb (II) uptake.

1. Introduction

Lead(II) is known toxic chemical species in water. High lead(II) concentration in drinking water is known to have adverse human health effects, such as anemia, kidney failure, mental retardation, and physiological defects [1]. Lead(II) in the aquatic environment may originate from mainly from anthropogenic activities. Many methods such as coagulation, chemical precipitation, solvent extraction, membrane separation, reverse osmosis, ion exchange, and adsorption have been used to remove heavy metals, including lead(II), from water and wastewater [2–4]. Among all of these methods, adsorption is a simple, effective, and inexpensive process for Pb(II) removal from dilute aqueous solutions [5]. Activated carbon, due to its large specific surface area, microporous structure, and stable chemical properties, has been widely used for environmental remediation practices including water purificaiton. Wood and coal are generally the major raw materials for activated carbon manufacturing. However, the availability of these raw materials has prompted several studies to use waste agricultural by-products for the removal of metals from water and wastewater [6–8]. Activated carbon has been reported effective in removing Pb(II) from wastewater [9–11]. Huang et al. [12–19,58] were among the early researchers to study the adsorption of heavy metals from water by commercial activated carbon. Imamoglu and Tekir [20] studied the removal of Cu(II) and Pb(II) from water using activated carbon prepared from hazelnut husks. Song et al. [21] reported effective removal of Pb(II) using a surface modified coconut-based activated carbon. While results of the above studies generally showed effective removal of lead from wastewater at high concentrations, Pb(II) removal at dilute concentration was rather inefficient. Therefore, absorbents with strong adsorption capability over an extended concentration range for metal removal from water are needed.

Iron oxide, with pH_{zpc} in the neutral pH range and capable of removing a wide group of cations and anions, has received considerable attention [22–24]. Raven et al. reported high adsorption capacity toward Pb(II), Cu(II), Zn(II), Ni(II), and Cr(VI) by iron-based adsorbents [25,26]. However, iron-based adsorbents had relatively small specific surface area, slow mass transfer, and low recycle/reuse potential [27]. Therefore; there are interests in activated carbon-iron oxide composites. Bagasse is a solid residue from the sugar cane refinery industry and can be a sustainable resource of material for the preparation of activated carbon [28].

In this study, we prepare a nano-hemite-bagasse composite (*n*-HBC)

* Corresponding author at: College of Light Industry and Food Engineering, Guangxi University, Nanning 530004, PR China.
** Corresponding author at: Department of Civil and Environmental Engineering, University of Delaware, Newark, DE 19716, United States.
E-mail addresses: wangdunqiu@sohu.com (D. Wang), huang@udel.edu (C.P. Huang).

https://doi.org/10.1016/j.jwpe.2017.11.014
Received 5 September 2017; Received in revised form 17 November 2017; Accepted 26 November 2017
Available online 07 December 2017

and study the Pb(II) adsorption characteristics of this material. Factors such as contact time, pH, Pb(II) concentration, and bagasse content on the metal adsorption capacity of *n*-HBC were studied first in batch experiments. Pb(II) adsorptipon characteristics on hydrous *n*-HBC described in terms of Langmuir adsorption isotherm and surface complex formation model.

2. Materials and methods

2.1. Materials

All chemicals/reagents used in the study were of analytical grade and used without further purification except lead standard solution. Ferric chloride hexahydrate ($FeCl_3{\cdot}6H_2O$), ammina ($NH_3{\cdot}H_2O$), sodium hydroxide (NaOH), nitric acid (HNO_3), lead nitrate ($Pb(NO_3)_2$), sodium chloride (NaCl) and cetyl-trimethyl ammonium bromide (CTMAB) were purchased from Country Medicine Group in Shanghai, China. Bagasse was obtained from a sugar industry site in Guangxi, China.

2.2. Preparation of n-HBC

First, bagasse was dried in an oven at 80 °C for 24 h then ground into small size and sieved to an average particle size of 5 mm. One mol/L of $FeCl_3$, 0.05 mol/L of (CTMAB) and 10% (v/v) of ammonia solution, all of analytical grade, were prepared with ultrapure water. Add CTMAB, (100 mL at 0.05 mol/L) and ultrapure water (800 mL) into a 2-L beaker and heated to boiling. Then, added 100 mL of 1 mol/L $FeCl_3$ solution to the boiling solution while slowly stirring to obtain a red-brown colloid solution. Mixed fifty gram dried bagasse with the colloid solution. After mixing for 24 h, the pH value of the mixture was adjusted to 7.4 with 10% (v/v) ammonia solution using an automatic potentiometric titrator (Metrohm 848 Titrino Plus) to produce bagasse–ferric hydroxide composite. The solid was filtered and dried in an oven at 105–110 °C for 24 h followed by drying in a muffle furnace to collect nano-$Fe(OH)_3$-bagsse solid, which was then carbonized/activated at 550 °C for 4 h to obtain *n*-HBC [29]. For the purpose of comparison, carbonized bamboo biochar without nnao-hematite was prepared. Briefly, the dried bamboo biochar (average particle size 5 mm) was heated at 550 °C for 4 h in a muffle furnace at a heating rate of 4 °C per min then allowed to cool to room temperature.

2.3. Batch adsorption experiments

Batch Pb(II) removal experiments were conducted first. A desired amount of *n*-HBC powder was weighted and put in a series of plastic centrifuge tubes (100 mL) and added 50 mL solution of different Pb(II) concentrations (i.e., 20–50 mg/L). After adjusting the pH, with NaOH (0.1 M) or HNO_3 (0.1 M), to pre-selected value the centrifuge tubes were sealed with capsules and placed on a temperature shaker (i.e., 25°, 35° or 45 °C) and shaken at a speed of 200 strokes per min to attain adsorption equilibrium. After centrifugation at 4000 rpm for 5 min, the supernatant was filtered through 0.45-μm micro-pore membrane and added 0.2% (V/V) HNO_3 to stabilize the sample in 100 mL volumetric flask before analyzing for the residual Pb(II). Samples were stored in acid-washed high-density polyethylene containers until analysis of residual Pb(II). All samples were analyzed within three days of collection.

The adsorption capacity of *n*-HBC at time, *t*, was calculated according to the mass balance relationship of Pb(II) ions expressed as:

$$q = \left(\frac{V}{X}\right) \times (C_o - C_t) \quad (1)$$

where C_0 and C_t are Pb(II) concentration (in mg/L) at initial and time *t*, respectively. *V* is the volume of the solution (L) and X is the mass of the *n*-HBC used (g). The percent Pb(II) removal, R, was determined by the following equation:

$$R(\%) = 100 \times \left(\frac{C_o - C_t}{C_o}\right) \quad (2)$$

2.4. Experimental conditions

The effect of various operating parameters, namely, contact time (30–1200 min), solution pH (2.0–9.0), adsorbent dosage (0.67-2.67 g/L), initial Pb(II) concentration (20–50 mg/L) and temperature (298–318 K), on Pb(II) adsorption were studied first. The adsorption isotherm, adsorption rate, and thermodynamic parameters at pH 5.0 were obtained and analyzed as well.

2.5. Surface characterization of n-HBC

Specific surface area was determined according to the Brunauer–Emmet–Teller (BET) equation by nitrogen gas adsorption using a Quantachrome Nova Station apparatus. Surface charge was determined by alkalimetric titration of 0.2 g/L solid suspension with NaOH (10^{-3} M) and HCl (10^{-3} M) in NaCl(10^{-2} M) as supporting electrolyte. The pH value was recorded using a pH meter, model PB-10 (Sartorius Co. Germany). Additionally, the zeta potential of the adsorbent was measured as a function of pH in NaCl(10^{-2} M) electrolyte using Nanoparticle & Zeta Potential Analyzer, model ZS90 (Malvern Co. England).

The structural feature of the *n*-HBC was observed using Hitachi S-4800 scanning electron microscope (SEM) at the acceleration voltage of 10 kV. Infrared spectra (FTIR) were obtained using KBr pellets (Acros, IR grade 99%, 1 mg of solid with 150 mg of KBr) with a Thermo Nicolet Nexus 470 Fourier transform spectrometer at 2 cm^{-1} resolution. X-ray diffraction (XRD) analysis on a X'Pert PRO X diffractometer using filtered copper Kα radiations. XPS experiments were performed with ESCALAB 250Xi using an Al Kα X-ray source (1486.6 eV). A nonlinear least-square curve-fitting program (XPSPEAK software 4.1, Raymund W. M. Kwork) was used to deconvolve the XPS data. Residual Pb(II) concentration was determined by atomic absorption spectrometer (Perkin Elmer AAnalyst 700).

3. Results and discussions

3.1. Surface characteristics of n-HBC

Fig. 1a shows the SEM images of *n*-HBC. The size and shape of nano-hematite particles on *n*-HBC could be seen from the SEM images. The size and shape of nano-hematite particles on *n*-HBC could be seen from the SEM images. The size of nano-hematite particles was in the range of 50 and 100 nm. Fig. 1b shows XRD spectra of *n*-HBC. All major peaks could be clearly seen and identified as standard hematite (α-Fe_2O_3) (00-033-0664), confirming the formation of hematite (α-Fe_2O_3) during preparation. Fig. 1c shows the FTIR spectra of *n*-HBC. The absorption peaks were at 3426, 2924, 2852, 1630, 1400, 1170, 1120 and 610 cm^{-1}, respectively. The =C=O functional groups were at 1630 cm^{-1} and −OH functional groups appeared at 3426 cm^{-1}. The peak at 2852 cm^{-1} was attributed to C−H stretching vibration. The peak at 1400 cm^{-1} was associated with −OH bending deformation in carbocyclic acids and phenolic groups. The adsorption band at 1170 cm^{-1} was asymmetric stretching of the C−O−C bridge. The peak at 1120 cm^{-1} was attributed to some overtones. The oxygen-containing functional groups were present abundantly on the external and internal surfaces of *n*-HBC, as adsorption sites and contributed to the adsorption capacity of *n*-HBC. The FTIR spectra of *n*-HBC were different from that of oxidized activated carbon reported by Ding et al. [30]. Ding et al. [30] reported that the peaks at 2338 cm^{-1} due to C≡C stretching and 1722 and 1595 cm^{-1} due to C=O stretching were reduced, and the peaks at 1061 cm^{-1} due to C−O stretching disappeared upon heating at 550 °C. They also suggested that heating at elevating temperature

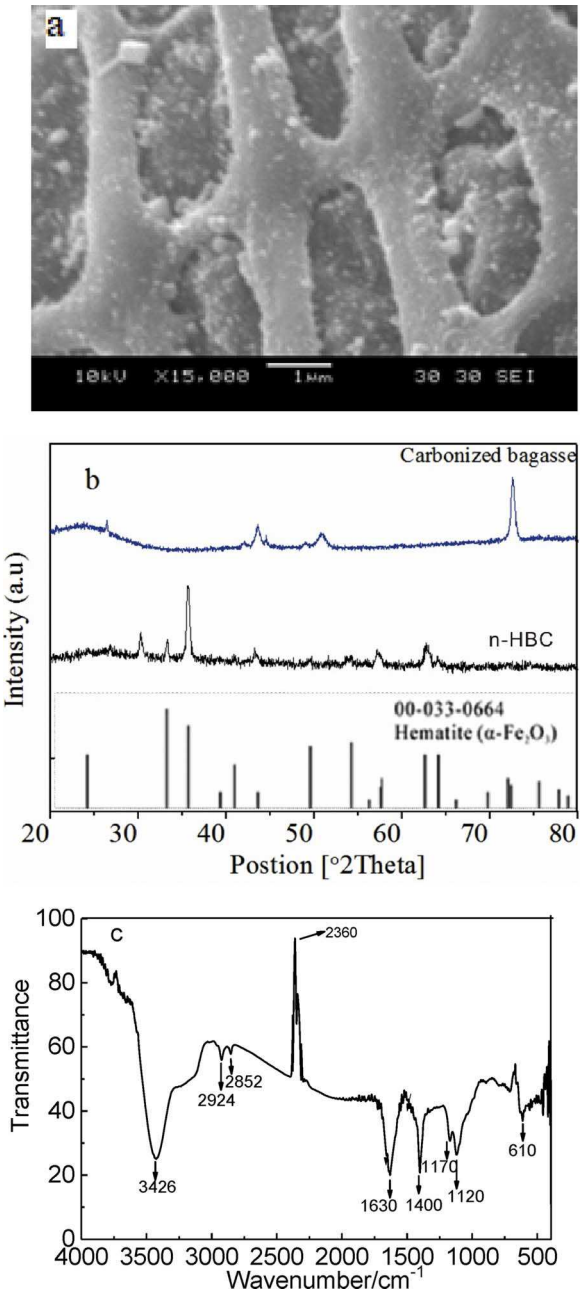

Fig. 1. Surface characterization of *n*-HBC. a. SEM, b. XRD, c. FTIR.

decreased the surface functional groups. The peak at 610 cm^{-1} was attributed to the Fe—O groups, proving the presence of Fe_2O_3 [31,32].

The specific surface area was 66.9 m^2/g determined by the BET N_2 adsorption method. "Ding et al. [30] prepared bagasse biochars at different temperature and reported specific surface area (mean geometric particle size 0.7 mm) of 0.56, 0.78, 1.98 and 14.1 m^2/g at heating temperature of 250, 400, 500, and 600 °C, respectively. In the absence of data for the specific surface area of carbonized biochar, based on the results reported by Ding et al. [30], a specific surface area of 7 m^2/g was estimated for the carbonized biochar. The large specific surface area of *n*-HBC can be attributed in part to the nano-size hematite particles on the biochar.

The average pore diameter and the total pore volume were 12.25 nm and 0.0201 cm^3/g, respectively, calculated by the BJH method.

Fig. S1 shows the zeta potential as a function of pH. From Fig. S1, the pH_{zpc} of *n*-HBC was 4.93.

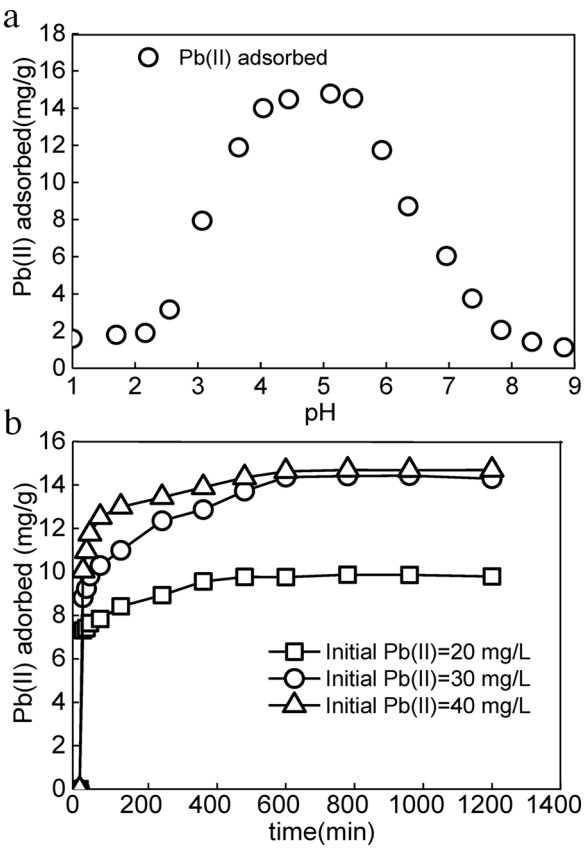

Fig. 2. Major factors affecting Pb(II) adsorption onto *n*-HBC, (a) final pH and (b) initial Pb (II) concentration. Experimental conditions: [*n*-HBC] = 2 g/L, Temperature = 25 °C. For (a) Co = 30 mg/L; for (b) pH = 5.

3.2. Major factors affecting Pb(II) adsoriton

The pH of the solution plays an important part on ion adsorption, because solution pH governs the distribution of both the adsorbent surface metal binding sites and the metal ions in water [33]. Fig. 2a shows the adsorption of Pb(II) on *n*-HBC as a function of pH. Results clearly indicated the importance of solution pH on Pb(II) adsorption [34]. When the pH value was increased from 1.0 to 5.0, the adsorption capacity was increased from 1.90 to 14.74 mg/g. The optimum pH for Pb(II) adsorption was found in the range from 4.0 to 5.5.

Obviously, the nature of the surface charge could play a role in Pb (II) adsorption [35]. At pH > pH_{zpc}, the adsorbent surface is negatively charged, which strong electrostatic attraction between the surface groups and Pb(II) species might occur [35]. *n*-HBC had a pH_{zpc} of 4.93 (Fig. S1), indicating a positive surface charge below pH 4.93. On the contrary, the surface of *n*-HBC was negatively charged at pH > pH_{zpc}. It is noted that at pH ~ pH_{zpc}, the predominant Pb(II) species was Pb^{2+}; other species such as $[Pb(OH)]^+$, $Pb(OH)_2$, and $[Pb(OH)_3]^-$ were present at pH > pH_{zpc} (Fig. S6). Strong intersection between the negatively charged *n*-HBC surface and cationic Pb^{2+} species was expected, although specific chemical adsorption could not be ruled out as important contributing forces for metal ion adsorption [18].

Fig. 2b shows the effect of contact time on Pb(II) adsorption. The residual Pb(II) concentration decreased rapidly at the onset of adsorption experiment, which was typical of ion adsorption from dilute aqueous solutions and indicative of favor interactions between *n*-FOBC and Pb(II). Results in Fig. 2b also show that the amount of Pb(II) adsorption reached a plateau at 480, 600, and 720 min at the initial Pb(II) concentration of 20, 30, and 40 mg/L, respectively, under experimental condition of 25 °C and pH 5.0. It was observed further that Pb(II) was adsorbed within the first 60 min at an average adsorption rate of

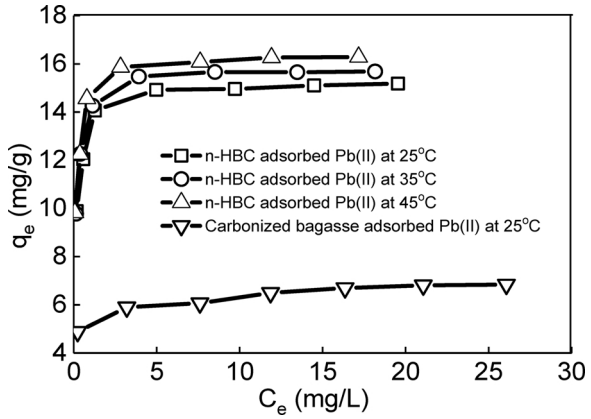

Fig. 3. Langmuir adsorption isotherm of Pb(II) on *n*-HBC at different temperature (Ionic strength = 10^{-2} M NaCl; pH = 5.0).

0.114 mg/g-min when the initial Pb(II) concentration was 20 mg/L, temperature at 25 °C and pH 5.0. A similar trend for initial Pb(II) concentration of 30 and 40 mg/L was also observed. There were reports that adsorption reaction occurred rapidly during the initial stage, which was followed by a slow reaction till equilibrium [36]. The presence of a large number of vacant sites at the initial stage may be the cause of raid initial uptake of adsorbate species [37].

3.3. Adsorption isotherm

Fig. 3 shows the Pb(II) adsorption isotherm for carbonized and *n*-HBC at different temperature, i.e., 25, 35 and 45 °C. The adsorption density increased with increase in temperature at specific initial Pb(II) concentration. The Pb(II) absorption density increased from 9.69 to 15.18, 9.78 to15.69, and 9.83–16.28 mg/g when the equilibrium Pb(II) concentration was increased from 0.20 to 20 mg/L, at 25 °C, 35 °C, and 45 °C, respectively. It is interesting to note that *n*-HBC exhibited a Pb(II) adsorption density three times that of carbonized bagasse.

The Pb(II) adsorption density can be described well by the Langmuir adsorption isotherm

$$q = \frac{q_m K_L C_e}{1 + K_L C_e} \tag{3}$$

Where, q, q_m, K_L, and C_e are adsorption density, monolayer-layer adsorption density, Langmuir constant, and equilibrium concentration, respectively. Results showed that the degree of data fitness by the Langmuir adsorption isotherm was good with correlation coefficient, R^2, of 0.9988, 0.9998, and 0.9998, at 25, 35, and 45 °C, respectively. The adsorption dsnsity increased from 16.57 at 25 °C to 17.24 mg/g at 45 °C. Results indicated that Pb(II) adsorption on *n*-HBC was endothermic. *n*-HBC exhibited a Pb(II) adsorption capacity of 16.6 mg/g, which was less than 40.1 mg/g of an acid oxidized commercial acticated carbon [30], slightly less than 17.82 mg/g of bamboo charcoal [38] and slightly greater than 15.96 mg/g of activated carbon prepared from Van apple pulp [19]. However, The Pb(II) adsorption density of *n*-HBC was much greater than 7.04 mg/g of carbonized bagasse at 25 °C. The K_L values were 6.10×10^7, 2.07×10^8, and 2.38×10^8 M^{-1} at 25 °C, 35 °C and 45 °C, respectively. The change of Gibbs free energy of adsorption, ΔG, can be calculated from the Nernst equation, $\Delta G = -RT \ln(K_L)$, where R is the gas constant (8.314 J/mol K) and T is the absolute temperature (K). The Gibbs free energy value (Table 1) indicated the spontaneous nature of adsorption.

3.4. Surface acidity of n-HBC

The surface acidity of hydrous solids is an important property contributing to interfacial interactions with ions. Upon hydration, the solid surface develops surface hydroxyl groups that behave amphoterically [39–41,20]:

$$\underline{S}O\ H_2^+ \Leftrightarrow SOH + H^+;\ K_{a2}^{int} \tag{4a}$$

$$\underline{S}O\,H \Leftrightarrow \underline{S}O^- + H^+;\ K_{a2}^{int} \tag{4b}$$

where $\underline{S}OH_2^+$, $\underline{S}OH$, and $\underline{S}O^-$ represent protonated, neutral, and depronated surface hydroxyl groups, respectively. The various surface hydroxyl groups formed may not be structurally and fully chemically homogeneous [39,42], but for the sake of simplicity a single hydroxyl group in the chemical reaction was considered. The deprotonated surface group $\underline{S}O^-$ behaves as a Bronsted base; whereas the protonated $\underline{S}OH_2^+$ group is a Bronsted acid. At constant ionic strength the surface activity or surface concentration of the surface species are assumed to be equal. The surface acidity of any hydrous solid canbe expressed in terms of acidity strength, i.e., intrinsic surface acidity constants, pK_{a1}^{int} and pK_{a2}^{int} and total surface site, N_t (μC/cm^2), which is the sum of the three surface hydroxyl groups, i.e.,

$$N_t = \{\underline{S}OH_2^+\} + \{\underline{S}OH\} + \{\underline{S}O^-\} \tag{5}$$

Based on alkalimetric titration and zeta potential measurement, it is possible to calculate the surface acidity of a hydrous solid such as *n*-HBC (Supporting Information, S4). As shown in the Supporting Information, The acidity constants, pK_{a1}^{int} and pK_{a2}^{int}, were 3.29 and 6.57, respectively and the acidity capacity, N_t, was 10.56 μC/cm^2 at ionic strength of NaCl(10^{-2} M). Based on the intrinsic acidity constants, it is possible to calculate the speciation of the *n*-HBC surface acidity (Supporting Information, S4). The surface and Pb(II) speciation canbe used to calculate the surface complex between Pb(II) and hydrous *n*-HBC.

3.5. Surface complex formation (SCFM)

At low metal concentration, metal adsorption onto hydrous solids such as metal oxides is mainly a surface coordination process that can be modeled thermodynamically as a complexation reaction between surface sites and adsorbates [43]. The surface complex formation model (SCFM) has been successfully used to describe the adsorption reactions at oxide-water interfaces [17,44–47] with excellent predictability. For the sake of simplicity, a SCFM originally proposed by Huang and Stumm [39] was employed to describe the adsorption of Pb(II) on *n*-HBC. Huang and coworkers have used this model to describe the adsorption of metal ions onto many adsorbates including γ-Al_2O_3 [39], metal sulfides [40,48], activated carbon [17,18], concrete materials [49], sludge particulates [50], and algal biomass [51].

Based on the above data, the following complex formation was proposed for the adsorption of Pb(II) onto hydrous *n*-HBC:

$$\underline{S}O^- + Pb^{2+} \rightarrow \underline{S}OPb^+;\ K_s = \frac{\{\underline{S}OPb^+\}}{\{\underline{S}O^-\}[Pb^{2+}]} \tag{6a}$$

or

$$\underline{S}OH + Pb^{2+} \rightarrow \underline{S}OPb^+ + H^+;\ K_s^* = \frac{\{\underline{S}OPb^+\}\{H^+\}}{\{\underline{S}OH\}[Pb^{2+}]} \tag{6b}$$

Table 1
Langmuir isotherm parameters for the Pb(II) adsorption on *n*-HBC at different temperature.

Item	Langmuir			ΔG (KJ/mol)
	q_m (mg-Pb)/g)	$K_L/(M^{-1})$	R^2	
Carbonized bagasse (25 °C)	7.04	4.9×10^7	0.9995	−39.49
(25 °C)	16.6	6.6×10^7	0.9988	−39.37
(35 °C)	16.9	2.1×10^8	0.9998	−47.50
(45 °C)	17.2	2.4×10^8	0.9998	−47.86

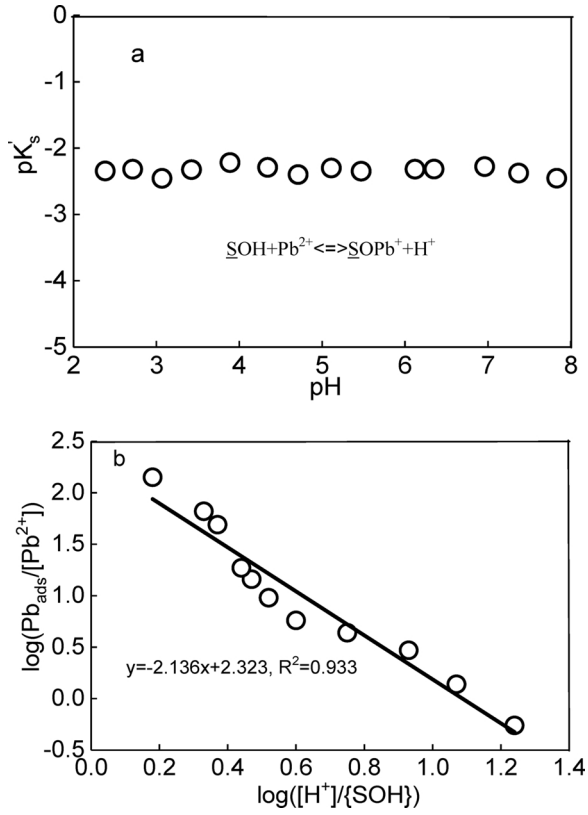

Fig. 4. Determine log K_s^*. (a) Calculated from Eq. (6c). (b) Kurbatov plot, $\log\left[\frac{pb}{[pb^{2+}]}\right]$ versus$\log\left[\frac{\{H^+\}}{\{SOH\}}\right]$ plot.

Note that the stability constant, K_s is related to K_s^* by the following relationship:

$$K_s^* = K_s \text{ x } K_{a2}^{int} \tag{6c}$$

The total amount of Pb(II) adsorbed, Γ_t (mol/g) was obtained directly from the adsorption experiment. The Pb(II) equilibrium concentration [Pb^{2+}] could be obtained from the mass balance relationships:

$$[Pb^{2+}] = \alpha_0\left(\frac{Pb_T}{W} - \Gamma_t\right) \tag{7}$$

where α_0 = fraction of Pb(II) specie at equilibrium; W(g/L) = mass concentration of *n*-HBC; Pb_T = total initial Pb(II) concentration (M). From the surface acidity parameters determined above, i.e., pK_{a1}^{int}, pK_{a2}^{int}, N_t, ψ_0, the total amount of metal adsorbed, Γ_t, and the distribution of Pb(II) species as a function of pH (Fig. S6), it is possible to calculate the stability constant of the surface lead (II) complex as a function of pH (Fig. 4a). The average stability constant was $\log K_s^*$ = 2.36. Furthermore, a plot of $\log\left[\frac{Pb_{ads}}{[Pb^{2+}]}\right]$ versus $\log\left[\frac{\{H^+\}}{\{SOH\}}\right]$, (i.e., Kurbatov plot) also yielded $\log K_s^*$ (from the intercept, Fig. 4b) value of 2.32, which was very close to the $\log K_s^*$ value determined in Fig. 4a above. Note that K_s* is pH dependent.

The stability constants, K_s, for Pb(II)-*n*-HBC complex was calculated from Eq. (6c), i.e., K_s and K_{a2}^{int}. The stability constant, $\log K_s$, was 8.89 at 25 °C. It must be noted that K_s is the same as the Langmuir adsorption constant, K_L. Results showed that K_s was in the same order of magnitude as K_L (Table 1). Weng [52] reported the formation of surface complexes, = $SOPb^+$ and = SOPb(OH) sandy loam soil surface with stability constants ($\log K_s$) of 4.2–4.7 and 7.1–7.3, respectively. Similar results were reported for the formation of surface complexes, = $SOCu^+$ and = SOCuOH, between Cu(II) and powdered pineapple leaves [59] and Cu(II) and black tea leave [60]. The stability constant between Pb^{2+} and *n*-HBC, was in the same order of magnitude as those reported by Weng [52]. Nonetheless, in the present work, there was no formation of =SOPb(OH) surface complex.

The Gibbs free energy of adsorption, ΔG_{ads}^0, can be determined by the Nernst equation:

$$\Delta G_{ads}^0 = 2.303 \text{ RT } pK_s \tag{8}$$

where R is the gas constant (8.314 J/K-mol or 1.986 cal/K-mol) and T is the absolute temperature (K), at pK_s = −8.89, the Gibbs free energy of adsorption was: ΔG_{ads} = −50.7 kJ/mol (or 12.1 kcal/mol), which was of the same order of magnitude as that calculated from the of the same order of magnitude as that calculated from the Langmuir adsorption constant, K_L, at 25 °C Weng and Huang reported ΔG_{ads}^0 value of −7.1 kcal/mol for the adsorption of Zn(II) onto fly ash [53]. Weng et al. reported ΔG_{ads}^0 value of −5.7 to −7.3 kcal/mol for the adsorption of Cu(II) onto spent activated clay [54]. The negative ΔG_{ads}^0 value indicated the spontaneuity of Pb(II) ion adsorption onto *n*-HBC.

3.6. Chemical nature of Pb(II) interaction with n-HBC

Fig. 5 shows the results of energy dispersive spectrometric (EDS) analysis. The atomic percentage of C, O and Fe of *n*-HBC was 33.22, 65.67, and 1.12%, or mass percentage of 25.22%, 68.47% and 4.07%, respectively. After Pb(II) adsorption, the atomic percentage of C, O and Fe was 31.02%, 65.44% and 3.40% and the mass percentage were 23.08%, 64.85%, and 11.76%%, respectively. The mass percentage of Pb(II) was 0.7%, which was the same as that based on the maximum adsorption capacity calculated by the Langmuir adsorption isotherm. This pattern showed the presence of Pb(II) peak, confirming the Pb(II) adsorption on *n*-HBC surface.

The major characteristic major peaks (2θ) of *n*-HBC before Pb(II) adsorption were at 33.37°, 35.63°, 57.16°, 43.15°and 62.95°, which were shifted to 33.29°, 35.60°, 43.28°, 57.32°and 63.03°, respectively, after pB(II) adsorption. The major peaks of carbonized bagasse were at 43.59° and 50.83° before Pb(II) adsorption. The peak at 50.83° disappeared after Pb(II) adsorption Pb(II), indicating the presence of oxygen-containing functional groups that were responsible for Pb(II) adsorption (Fig. 6).

Fig. 7 shows the deconvoluted XPS spectra of O 1s, C 1s and Fe 2p orbitals. The C1s signal at 284.8 eV was assigned to hydrocarbon contamination. This peak was taken as reference. No shift of XPS spectra of C1s, C−C, C=C and C=O suggested that carbon species was not involved in adsorption process. The main O1s peak was shifted from 531.8 eV to 532.1 eV after Pb(II) adsorption. Results showed the presence of oxygen-containing functional groups on the surface of −HBCin the form of carboxyl oxygen, −O−C=O (533.4 eV), and carbonyl oxygen, =O=C (530.6 eV). Pb (II) adsorption was accompanied by a change in oxygen bonding, providing evidence that oxygen-containing functional groups took part in Pb (II) adsorption. The bonding energy of Fe 2p was increased from 710.8 to 710.9 eV after Pb(II) adsorption; these values were typical for Fe(III) in Fe_2O_3.

The bonding energy change reflected electron transfer in the valence band. In fact, the actual charge transfers due to chemical reactions occurred. Therefore, by tracking the change in core level peak position of the substrate with and without formation of surface complexes, it is possible to deduce the direction of electron transfer during adsorption and to assess the relative acidity and basicity of substrate and adsorbate [55].

The O1s binding energy and intensity shift was dependent on the content of different oxygen atoms, in particular on the surface of *n*-HBC. A simple formula connecting O1 s chemical shift and charge has been constructed with frontier molecular orbital theory as the theoretical framework [56]:

$$Q_o = -4.372 + \frac{385.023 - 8.976 \times (545.509 - O1sBE)^{1/2}}{4.488} \tag{9}$$

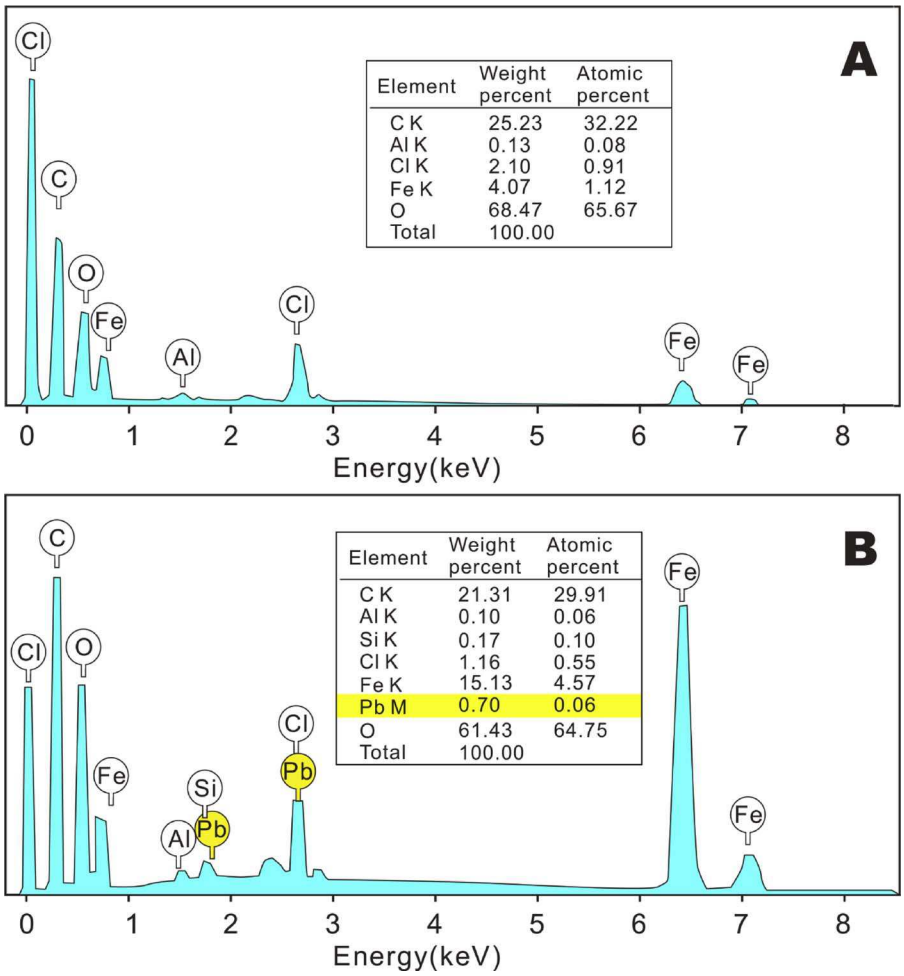

Fig. 5. Surface composition of *n*-HBC by EDS analysis. (a) Before Pb(II) adsorption; (b) After Pb(II) adsorption.

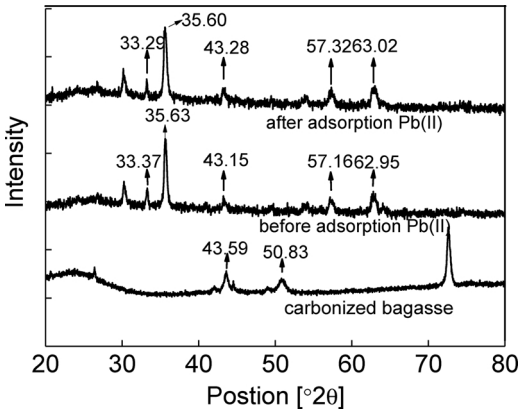

Fig. 6. XRD spectrum of *n*-HBC.

where Q_0 is the actual oxygen charge in sorbent and O1 s BE is the O1 s binding energy determined from XPS.

Moulder et al. [57] reported that the Q_0 value of metal oxides was between 533.6 and 528.3 eV. The O1s binding energy and the actual charge of oxygen of surface oxygen groups should also be compatible with the migration of iron binding energy. Iron charge can be calculated from iron atom core level XPS analysis and as following [56]:

$$Q_{Fe} = 0.3233BE_{Fe2p} - 228.51 \quad (10)$$

where Q_{Fe} is the actual charge of iron, BE_{Fe2p} is the binding energy obtained by XPS analysis.

According to Eq. (9), the charge of oxygen of *n*-HBC surface before and after Pb(II) adsorption were −0.80 and −0.81 esu, respectively. It indicated that before and after Pb(II) adsorption, the actual charge of oxygen of surface species was insignificantly changed, which indicated that Pb(II) adsorption on *n*-HBC did not involve noticeable electron transfer between *n*-HBC surface and Pb (II).

According to Eq. (10), the charge of surface iron species before and after Pb(II) adsorption were 1.29 and 1.32 esu, respectively. It indicated that charge of surface iron species was slightly changed after Pb(II) adsorption, which was correspondent to the actual charge of O 1s. After Pb(II) adsorption, the iron charge became more positively charged, suggesting that the surface iron atoms acted as Lewis base in the adsorption of Pb^{2+}, which was a Lewis acid. The results agreed with the above context that Pb(II) adsorption on *n*-HBC formed surface complex, −SO-Pb^{+}.

Fig. 8 shows the XPS spectra of Pb 4f, $Pb4f_{5/2}$, and $4f_{7/2}$ orbitals. The peak Pb 2f shifted from the reference binding energy of 137.6–142.4 eV [57]. The $Pb4f_{5/2}$ peak at 138.9 eV and the Pb $4f_{7/2}$ peak at 143.8 eV were clearly seen. The shift of Pb 4f orbital spectra at the binding energy(BE) of 137.5 eV after Pb(II) absorption demonstrated clearly that the surface oxygen-containing functional groups were involved in the adsorption reaction and that hematite played a significant role on Pb(II) adsorption.

3.7. Engineering implications

Results clearly show the merits of the *n*-HBC as an adsorbent for the removal of trace metals such as Pb(II) from water. From the engineering process applications point of view, this adsorbent has three major attributes. First, the nan-hematite particles contribute great specific

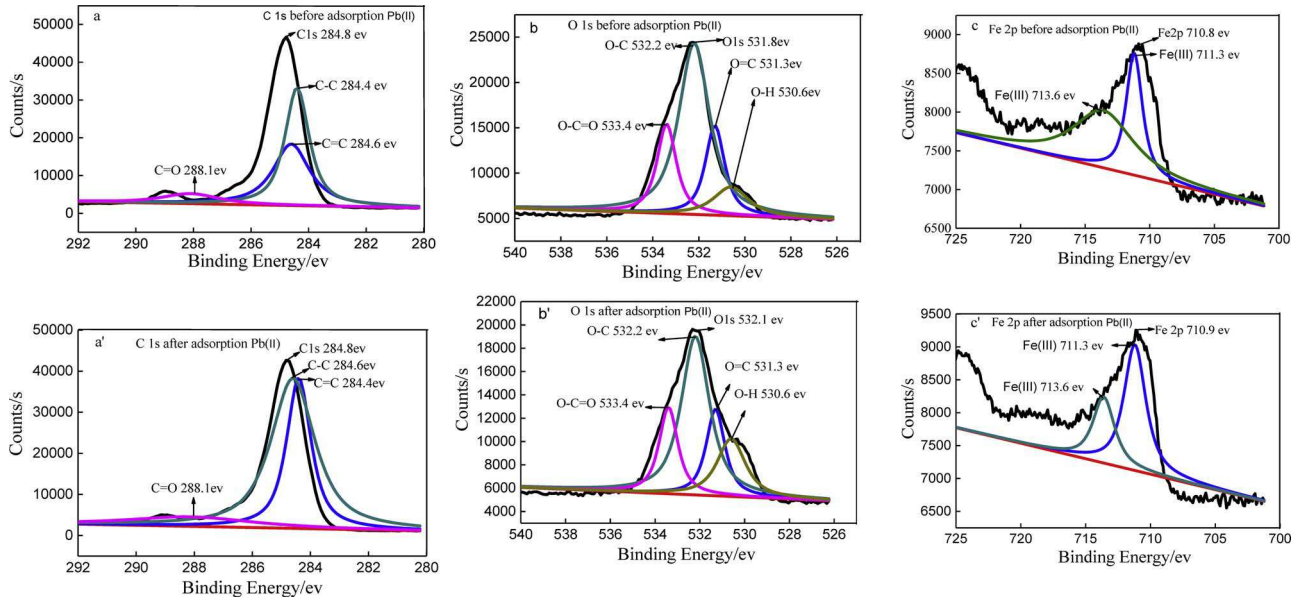

Fig. 7. XPS spectra of *n*-HBC before and after Pb(II) adsorption. (a): C 1s; (b): O 1s; (c): Fe 2p.

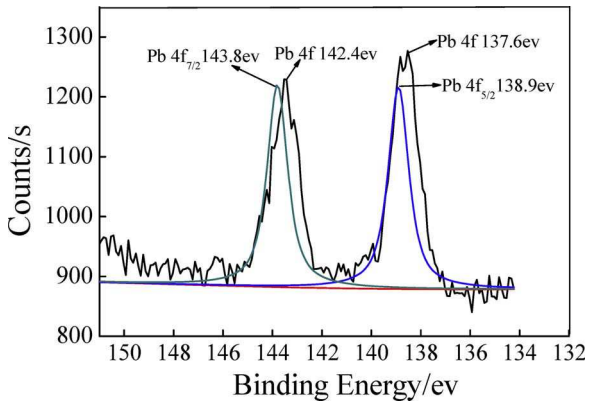

Fig. 8. The XPS spectra of Pb on *n*-HBC before and after Pb(II) adsorption.

surface area to the *n*-BC, which provides major surface sites necessary for metal ion adsorption. Second, the bagasse support enables the design of the metal removal processes in the mode of fixed bed operation, which can greatly reduce the post-metal treatment costs of particle separation. Finally, the pH-dependent nature of metal adsorption enables easy regeneration of the saturated adsorbent. It is extremely feasible to regenerate the *n*-HBC when it reaches maximum metal adsorption capacity. For example, at pH < 2 and > 9, the Pb(II) adsorption capacity of *n*-HBC is small, which makes it easy to desorb Pb (II) from the surface. The Pb(II) concentration in the acid or base regenerating solutions is high, which makes it easy to recover Pb(II) and water.

4. Conclusion

The particle size of *n*-Fe_2O_3 was between 100 and 300 nm. Major oxygen-containing functional groups were present abundantly on the external and internal surfaces of *n*-HBC. The surface acidity constants of *n*-FOBC were $pK_{a1}^{int} = 3.29$, and $pK_{a2}^{int} = 6.57$ at 10^{-2} M of NaCl solution and 25 °C. The pH played a major role on Pb(II) adsorption onto hydrous *n*-HBC surface. The optimum pH for Pb(II) adsorption was in the range of 4.0–5.5 with maximum Pb(II) removal at pH 5.0. Pb(II) adsorption was fast with equilibrium time of 480, 600, 720 min, at 25 °C and pH 5.0, when the initial Pb(II) concentration was 20, 30, and 40 mg/L, respectively. The maximum adsorption capacity calculated from the Langmuir isotherm was 16.57 mg/g at 25 °C. Surface complexation model was able to satisfactorily describe the adsorption reaction between aqueous Pb^{2+} and *n*-HBC surfaces. The Gibbs free adsorption of adsorption was in the range of −39.73 and −50.72 kJ/mol, which indicated favorable Pb^{2+} adsorption onto *n*-HBC. The shift of Pb 4f orbital spectra at the binding energy(BE) of 137.5 eV after Pb(II) absorption demonstrated clearly that the surface oxygen-containing functional groups were involved in the adsorption reaction and that hematite played a significant role on Pb(II) adsorption. Under the context of surface complex formation supported by XS analysis, it was clear that the surface of *n*-HBC behaved as Lewis base and Pb(II), specifically Pb^{2+}, was Lewis acid in the adsorption of Pb(II) onto the *n*-HBC.

Acknowledgments

This paper has greatly benefited from the insightful comments of two anonymous reviewers. This research was financially assisted by the National Natural Science Foundation of China (NSFC21367010, NSFC51638006), Addition support was provided by US NSF IOA (1632899) to CPH.

Appendix A. Supplementary data

Supplementary data associated with this article can be found, in the online version, at https://doi.org/10.1016/j.jwpe.2017.11.014.

References

[1] J. Cruz-Olivares, C. Pérez-Alonso, C. Barrera-Díaz, F. Urēna-Nūnez, M.C. Chaparro-Mercado, B. Bilyeu, Modeling of lead (II) biosorption by residue of allspice in a fixed-bed column, Chem. Eng. J. 228 (2013) 21–27.
[2] O. Gok, A. Ozcan, B. Erdem, A.S. Ozcan, Prediction of the kinetics, equilibrium and thermodynamic parameters of adsorption of copper(II) ions onto 8-hydroxy quinoline immobilized bentonite, Colloids. Surf. 317 (2008) 174–180.
[3] M.K. Aroua, S.P.P. Leong, L.Y. Teo, C.Y. Yin, W.M.A.W. Daud, Real-time determined activated carbon using ion selective electrode, Bioresour. Technol. 995 (2008) 786–5792.
[4] R.M. Novais, L.H. Buruberri, M.P. Seabra, J.A. Labrincha, Novel porous fly-ash containing geopolymer monoliths for lead adsorption from wastewaters, J. Hazard. Mater. 318 (2016) 631–640.
[5] D.H. Chen, S.S. Banerjee, Fast removal of copper ions by gum arabic modified magnetic nano-adsorbent, J. Hazard. Mater. 147 (2007) 792–799.
[6] L. Largitte, P. Lodewyckx, Studying different methods to determine the thermo kinetic constants in the adsorption of Pb^{2+} on an activated carbon from Bois carré

seeds, J. Environ Chem. Eng. 2 (2014) 788–795.
[7] M. Momčilović, M. Purenović, A. Bojić, A. Zarubica, M. Ranđelović, Removal of lead(II) ions from aqueous solutions by adsorption onto pine cone activated carbon, Desalination 276 (2011) 53–59.
[8] K. Wantala, S. Sthiannopkao, B. Srinameb, N. Grisdanurak, K.W. Kim, Synthesis and characterization of Fe-MCM-41 from rice husk silica by hydrothermal technique for arsenic adsorption, Environ. Geochem. Health. 32 (2010) 261–266.
[9] L.V.A. Gurgel, O.K. Júnior, R.P.D.F. Gil, L.F. Gil, Adsorption of Cu(II), Cd(II), and Pb (II) from aqueous single metal solutions by cellulose and mercerized cellulose chemically modified with succinic anhydride, Bioresour. Technol. 99 (2008) 3077–3083.
[10] T. Depci, A.R. Kul, Y. Önal, Competitive adsorption of lead and zinc from aqueous solution on activated carbon prepared from Van apple pulp: study in single-and multi-solute systems, Chem. Eng. J. 200-202 (2012) 224–236.
[11] G.H. Xiu, P. Li, Prediction of breakthrough curves for adsorption of lead(II) on activated carbon fibers in a fixed bed, Carbon 38 (2000) 975–981.
[12] C.P. Huang, M.H. Wu, The removal of chromium(VI) from dilute aqueous solution by activated carbon, Water Res. 11 (1977) 673–679.
[13] C.P. Huang, A.R. Bowers, Use of activated carbon for Cr(VI) removal, Prog. Water Technol. 10 (5) (1978) 45–78.
[14] C.P. Huang, F. Ostovic, Removal of Cd(II) by activated carbon adsorption, J. Environ. Eng. ASCE 104 (5) (1978) 863–878.
[15] C.P. Huang, D. Blankenship, The removal of mercury(II) from dilute aqueous solutions by activated carbon, Water Res. 18 (1) (1984) 37–46.
[16] C.P. Huang, P.L.K. Fu, Treatment of arsenic(V)-containing water by the activated carbon Process, J. Water Pollut. Contr. Fed 1 (1984) 233–242.
[17] O.M. Coracioglu, C.P. Huang, the surface acidity and characterization of some commercial activated carbons, Carbon 25 (1987) 569–578.
[18] O.M. Coracioglu, C.P. Huang, The adsorption of heavy metals onto hydrous activated carbon, Water. Res. 21 (9) (1987) 1031–1044.
[19] C.P. Huang, L.M. Vane, Enhancing arsenic (V) removal by a Fe2 + treated activated carbon, J. Water Pollut. Control Fed 61 (9) (1989) 1596–1603.
[20] M. Imamoglu, O. Tekir, Removal of copper (II) and lead (II) ions from aqueous solutions by adsorption on activated carbon from a new precursor hazelnut husks, Desalination 228 (2008) 108–113.
[21] X.L. Song, H.Y. Liu, L. Cheng, Y.X. Qu, Surface modification of coconut-based activated carbon by liquid-phase oxidation and its effects on lead ion adsorption, Desalination 255 (2010) 78–83.
[22] H. Zeng, M. Arashiro, D.E. Giammar, Effects of water chemistry and flow rate on arsenic removal by adsorption to an iron oxide-based sorbent, Water. Res. 42 (2008) 4629–4636.
[23] E. Deliyanni, T.J. Bandosz, Importance of carbon surface chemistry in development of iron–carbon composite adsorbents for arsenate removal, J. Hazard. Mater. 186 (2011) 667–674.
[24] K. Wantala, E. Khongkasem, N. Khlongkarnpanich, S. Sthiannopkao, K.W. Kim, Optimization of As(V) adsorption on Fe-RH-MCM-41-immobilized GAC using Box–Behnken design: effects of pH, loadings, and initial concentrations, Appl. Geochem. 27 (2012) 1027–1034.
[25] K.P. Raven, A. Jain, R.H. Loeppert, Arsenite and arsenate adsorption on ferrihydrite kinetics, equilibrium, and adsorption envelopes, Environ. Sci. Technol. 32 (1998) 344–349.
[26] A. Jain, K.P. Raven, R.H. Loeppert, Arsenite and Arsenate adsorption on ferrihydrite: surface charge reduction and net OH-release stoichiometry, Environ. Sci. Technol. 33 (1999) 1179–1184.
[27] S. Yean, L. Cong, C.T. Yavuz, J.T. Mayo, W.W. Yu, V.L. Colvin, M.B. Tomson, Effect of magnetite particle size on adsorption and desorption of arsenite and arsenate, J. Mater. Res. 20 (12) (2005) 3255–3264.
[28] H. Boussarsar, B. Rogé, M. Mathlouthi, Optimization of sugarcane bagasse conversion by hydrothermal treatment for the recovery of xylose, Bioresour, Technol. 100 (2009) 6537–6542.
[29] Y.N. Zhu, M.N. Liang, R.R. Lu, H. Zhang, Z.J. Zhu, S.H. You, J. Liu, H.L. Liu, Phosphorus removal from aqueous solution by the Fe (III)-impregnate adsorbent prepared from sugarcane bagasse, Fresenius. Environ. Bull. 20 (5) (2011) 1288–1296.
[30] W. Ding, X. Dong, I.M. Ime, B. Gao, L.Q. Ma, Pyrolytic temperatures impact lead sorption mechanisms by bagasse biochars, Chemosphere 105 (2014) 68–74, http://dx.doi.org/10.1016/j.chemosphere.2013.12.042.
[31] L.Y. Feng, M.H. Cao, X.Y. Ma, Y.S. Zhu, C.W. Hu, Superparamagnetic high-surface-area Fe_3O_4 nanoparticles as adsorbents for arsenic removal, J. Hazard. Mater. 217-218 (2012) 439–446.
[32] A.O.A. Tuna, E. Ozdemir, E.B. Simsek, U. Beker, Removal of As(V) from aqueous solution by activated carbon-based hybrid adsorbents: impact of experimental conditions, Chem. Eng. J. 223 (2013) 116–128.
[33] P. Waranusantigul, P. Pokethityook, M. Kruatrachue, Kinetics of basic dye (methylene blue) biosorption by giant duckweed (Spirodela polyrrhiza), Environ. Pollut. 125 (2003) 385–392.
[34] G. Crini, Kinetic, equilibrium studies on the removal of cationic dyse from aqueous solution by adsorption onto a cyclodextrin polymer, Dyes. Pigm. 77 (2008) 415–426.
[35] K.G. Sreejalekshmi, K.A. Krishnan, T.S. Anirudhan, Adsorption of Pb(II) and Pb(II)-citric acid on sawdust activated carbon: kinetic and equilibrium isotherm studies, J. Hazard. Mater. 161 (2009) 1506–1513.
[36] P.C. Brandão, T.C. Souza, C.A. Ferreira, C.E. Hori, L.L. Romanielo, Removal of petroleum hydrocarbons from aqueous solution using sugarcane bagasse as adsorbent, J. Hazard. Mater. 175 (2010) 1106–1112.
[37] D. Kavitha, C. Namasivayam, Experimental and kinetic studies on methylene blue adsorption by coir pith carbon, Bioresour. Technol. 98 (2007) 14–21.
[38] M. Salman, M. Athar, U. Farooq, S. Rauf, U. Habiba, A new approach to modification of an agro-based raw material for Pb (II) adsorption, Korean J. Chem. Eng. 31 (3) (2014) 467–474.
[39] C.P. Huang, W. Stumm, Adsorption of cations on hydrousAl_2O_3, J. Colloid Interface Sci. 43 (2) (1973) 409–420.
[40] S.W. Park, C.P. Huang, The surface acidity of hydrous CdS (s), J. Colloid Interface Sci. 117 (2) (1987) 431–441.
[41] C.H. Weng, C.P. Huang, H.E. Allen, P.F. Sanders, Cr(VI) Adsorption onto hydrous concrete particles from groundwater, J. Environ. Eng. 127 (12) (2001) 1124–1131.
[42] W. Stumm, Chemistry of the Solid-water Interface: Processes at the Mineral-water and Particle-water Interface in Natural Systems, New York, Wiley, 1992.
[43] R.O. James, T.W. Healy, Adsorption of hydrolyzable metal ions at the oxide-water interface: III: A thermodynamic model of adsorption, J. Colloid Interface Sci. 40 (1) (1972) 65–81.
[44] B.E. Reed, M.R. Matsumoto, Modeling Cd adsorption in single and binary adsorbent (PAC) systems, J. Environ. Eng. 119 (2) (1993) 332–348.
[45] C.D. Cox, M.M. Ghosh, Surface complexation of methylated arsenates by hydrous oxides, Water Res. 28 (5) (1994) 1181–1188.
[46] C. Tiffreau, J. Lzenkirchen, P. Behra, Modeling the adsorption of mercury(II) on (hydr)oxides I: amorphous iron oxide and α-Quartz, J. Colloid Interface Sci. 172 (1995) 82–93.
[47] O.J. Hao, C.P. Huang, Adsorption characteristics of fluoride onto hydrous alumina, J. Environ. Eng. 112 (6) (1986) 1054–1069.
[48] S.W. Park, C.P. Huang, Chemical substitution reaction between Cu(II) and Hg(II) and hydrous CdS(s), Water. Res. 23 (12) (1989) 1527–1534.
[49] C.H. Weng, C.P. Huang, H.E. Allen, P.F. Sanders, Chemical interactions between Cr (VI) and hydrous concrete particles, Environ. Sci. Technol. 30 (2) (1996) 371–376.
[50] C.P. Huang, J.M. Wang, Specific chemical interactions between metal ions and biological solids exemplified by sludge particulates, Bioresour. Technol. 160 (2014) 32–42.
[51] C. Huang, C.P. Huang, A.L. Morehart, Proton competitive in Cu(II) adsorption by fungal mycelia, Water Res. 25 (11) (1991) 1365–1375.
[52] C.H. Weng, Modeling Pb(II) adsorption onto sandy loam soil, J. Colloid Interface Sci. 272 (2) (2004) 262–270.
[53] C.H. Weng, C.P. Huang, Adsorption characteristics of Zn(II) from dilute aqueous solution by fly ash, Colloids Surf., A 247 (1-3) (2004) 137–143.
[54] C.H. Weng, C.Z. Tsai, S.H. Chu, Y.C. Sharma, Adsorption characteristics of copper (II) onto spent activated clay, Sep. Purif. Technol. 54 (2) (2007) 187–197.
[55] M.B.H.W. Ding, B.H.W.S. De Jong, S.J. Roosendaal, A. Vredenberg, XPS studies on the electronic structure of bonding between solid and solutes: adsorption of arsenate, chromate, phosphate, Pb^{2+}, and Zn^{2+} ions on amorphous black ferric oxyhydroxide, Geochimca et Cosmochim Acta. 64 (7) (2000) 1209–1219.
[56] B.H.W.S. De Jong, D. Ellerbroek, Low-temperature structure of lithium nesosilicate, Li_4SiO_4, and its Li_{1s} and O_{1s} X-ray photoelectron spectrum, Acta Crystallogr. Sect. B: Struct. Sci. 50 (1994) 511–518.
[57] J.F. Moulder, W.F. Stickle, P.E. Sobol, K.D. Bomben, Handbook of X-ray Photoelectron Spectroscopy: a Reference Book of Standard Spectra for Identification and Interpretation of XPS Data, Physical Electronics, Eden Prairie, 1995.
[58] C.P. Huang, M.H. Wu, Chromium removal by carbon adsorption, J. Water Pollu. Contr. Fed. 47 (10) (1975) 2437–2446.
[59] C.H. Weng, Y.C. Wu, Potential low-cost biosorbent for copper removal: pineapple leaf powder, J. Environ. Eng.-ASCE 138 (3) (2012) 286–292.
[60] C.H. Weng, Y.T. Lin, D.Y. Hong, Y.C. Sharma, S.C. Chen, K. Ripathi, Effective removal of copper ions from aqueous solution using base treated black tea waste, Ecol. Eng. (2014) 127–133.